Late Pleistocene to Holocene tephrostratigraphic record from the Northern Ionian Sea

Late Pleistocene to Holocene tephrostratigraphic record from the Northern Ionian Sea

Caron B.[1,2], Siani G.[1], Sulpizio R.[3,4], Zanchetta G.[2,5,6], Paterne M.[7], Santacroce R.[2], Tema E.[8,9], Zanella E.[8,9], Dewilde F.[7]

[1]Laboratoire des Interactions et Dynamique des Environnements de Surface (IDES), UMR *8148, CNRS-Université de Paris-Sud, Bât 504, 91405 Orsay Cedex, France*
[2]*Dipartimento di Scienze della Terra, Via S. Maria 53, 56126 Pisa, Italy*
[3] *CIRISIVU, c/o Dipartimento Geomineralogico, via Orabona 4, 70125, Bari, Italy*
[4]*IDPA-CNR, via Mario Bianco 9, 20131, Milano, Italy*
[5]*IGG-CNR Via Moruzzi, 1, 56100, Pisa, Italy*
[6]*INGV-Pisa, Via della Faggiola, 32, 56126 Pisa, Italy*
[7] *Laboratoire des Sciences du Climat et de l'Environnement, Laboratoire Mixte CNRS-CEA - UVSQ, Avenue de la Terrasse 91198 Gif-sur-Yvette Cedex, France*
[8] *Dipartimento di Scienze della Terra, Via Valperga Caluso 35, 10125 Torino, Italy*
[8] *ALP, Alpine Laboratoryt of Paleomagnetism, 12016 Peveragno, Italy*

ABSTRACT

A detailed tephrostratigraphy study supported by stable isotope ($\delta^{18}O$) analyses and AMS ^{14}C dating was carried out on a high sedimentation rate deep-sea core recovered in the northern Ionian Sea. Eight tephra layers were recognized, all originated from explosive eruptions of southern Italian volcanoes. These tephra layers are correlated with terrestrial proximal counterparts and with both marine and lacustrine tephra already known in the central Mediterranean area. The oldest tephra (dated at ca. 19.4 ka cal BP) is tentatively correlated to the Monte Guardia eruption from Lipari Island. Two other rhyolitic tephra layers were correlated with the explosive volcanic activity of Lipari island: Gabellotto-Fiumebianco/E-1 (8.3 ka cal BP) located close to the interruption of Sapropel S1 deposit, and Monte Pilato (ca. AD 1335) in the uppermost part of the core. The Na-phonolitic composition of the other five recognized tephra layers indicates the Somma-Vesuvius as the source. The composition is quite homogeneous among the five tephra layers, and fits that of the Mercato proximal deposits. Beyond the striking chemical similarity with the Mercato eruption, these tephra layers spans over ca. 2000 years, preventing correlation with the single well known Plinian eruption of the Somma-Vesuvius. Therefore, at least two of these tephra layers were assigned to an interplinian activity of the Somma-Vesuvius between the eruptions of Mercato and Avellino, even though these eruptions remains poorly constrained in the proximal area. By contrast, the most prominent tephra layer (2 mm white tephra visible at naked eyes) was found within the S1a Sapropel interval. Despite the possible complication for the presence of similar eruption with different ages we argue that Mercato is probably a very good marker for the onset of sapropelic condition in the Ionian Sea and can be used for land-sea correlations for this important climatic event. More in general, these data allow a significant update of the knowledge of the volcanic ash dispersal from Lipari and Somma-Vesuvius volcanoes.

Keywords: tephrochronology, Ionian Sea, Somma-Vesuvius, Mercato, Lipari, Gabellotto-Fiumebianco/E-1, Monte Pilato, Monte Guardia

1. Introduction

The central Mediterranean region represents one of the most suitable area for tephrostratigraphic studies, owing to the frequent explosive activity of its volcanoes during Quaternary (e.g Keller et al., 1978; Thunell et al., 1979; McCoy, 1981; Paterne et al., 1988, 2008; Wulf et al., 2004; Margari et al., 2007). Over the last decades, marine tephra studies in this area have allowed to significantly improve the reconstruction of the explosive activity of the Mediterranean volcanoes (e.g. Keller et al., 1978; Paterne et al., 1986, 1988, 1990, 2008; Siani et al., 2004; Lowe et al., 2007; Margari et al., 2007; Turney et al., 2008; Bourne et al., 2010). In addition to their interest for volcanology, the identification of tephra layers on land and/or in the marine sediments have supplied a significant stratigraphic support to paleoclimatic and paleoceanographic investigations in this basin, improving chronology and correlation of marine, continental, and cryospheric records at ultra-regional scale (e.g. Paterne et al. 1986; Siani et al., 2001; Lane et al., 2010).

The Tyrrhenian, Adriatic and Ionian seas are the best studied basins of the Mediterranean area because of prevailing seasonal wind directions that mainly dispersed ash particles to the east and southeast, at least for the last 200 ka (Keller et al., 1978; Paterne et al., 1998, 2008; Siani et al., 2004; Bourne et al., 2010). However, the inspection of the location of the published cores shows an evident lack of data in the north part of the Ionian Sea. This creates a gap in the tephrostratigraphic network among the different marine basins and continental archives to retrace and provide new insight in the past explosive volcanic activity in the central Mediterranean area. In order to fill this gap, we selected a high sediment accumulation rate deep-sea core located in the northern Ionian Sea (MD 90-918; Fig. 1) for

detailed tephrostratigraphic studies. The ages of the marine tephra have been obtained through accelerator mass spectrometry (AMS) ^{14}C dating coupled to oxygen isotope measurements performed on monospecific planktonic foraminifera. The origin of the tephra layers were assessed by comparing major element compositions (SEM-EDS analyses), age estimates and morphological characteristics of vitric fragments with those of corresponding subaerial pyroclastic deposits. Here, an evaluation and refinement of the dispersal areas of some of the recognized eruptions is presented, in view to providing a contribution for the improvement of volcanic hazard assessment in the central Mediterranean area.

2. Material and analytical methods

2.1. Core lithology

Core MD 90-918 was recovered in the northern Ionian Sea (39° 35,64 N, 18°5 0,43 E; 695 m water depth, 14.77 m core length; Fig. 1) during the 1990 PROMETE II cruise of the French N/O Marion Dufresne. Grey hemipelagic ooze dominates the core lithology except for a 20 cm thick sandy layer centred at 992 cm depth representing a turbidite deposit (Fig. 2). A black-grey layer in the upper part of the core (between 204 and 231 cm depth), is referred to the Sapropel S1 deposit. This layer was deposited during the most recent period of stagnation in the East Mediterranean Sea (e.g. Kallel et al., 1997; Rohling et al., 1997, Mercone et al., 2000) and is marked by two black-grey beds (i.e. S1a and S1b) separated by a thin horizon of white hemipelagic ooze between 210 and 219 cm depth (Fig. 2).

2.2 Detection and chemical analysis of tephra

The core MD 90-918 was sampled at 5 cm interval for its entire length, with the exception of the Sapropel S1 deposit (between 204 and 231 cm) that was sampled at 1 cm interval, for recognition of volcanic particles. Each sample was then washed and sieved in the

fraction > 40 μm. Tephra layers are then defined by the relative abundance of volcanic glass shards with respect to detrital crystals and lithics in the same fraction after counting of at least 400 particles under a stereo-microscope. Volcanic glass occurs throughout the core, and forms a background at about 4 % of abundance for the 323 counted samples (Fig. 2). Therefore, we considered only abundance peaks larger than two times the background as representative of tephra deposition and selected for laboratory analyses. Glass shards and/or micropumice fragments were morphologically and lithologically described under stereo-microscope, then hand-picked and mounted on epoxy resin beads and polished in order to avoid compositional variations due to surface alteration processes.

Two different facilities were used to analyse the major element composition of micropumices and/or glass shards: the CAMECA-SX 100 Electron Probe Micro-Analyser (EPMA-CAMPARIS) available at the University Pierre et Marie Curie of Paris, (France) and the Philips SEM 515 device equipped with an EDAX-DX micro-analyser (SEM-DST) available at Dipartimento di Scienze della Terra (University of Pisa, Italy). Working conditions of EPMA-CAMPARIS comprise an acceleration voltage of 15 kV and a beam current of 4 nÅ. Usually, analytical data show closures > 97 wt. %, which indicate a limited or absent alteration of analysed glasses. Working conditions of SEM-DST were 20 kV acceleration voltage, 100 s live time counting, 1 nÅ beam current, 20-10 μm beam diameter, 2100 shots per second, ZAF correction. The ZAF correction procedure does not include natural or synthetic standards for reference, and requires the analyses normalization at a given value (which is chosen at 100 %).

The variance of analytical precision between the two instruments was calculated using the mean of the analyses from 5 tephra layers recognized along the core. The analysis indicates that the difference in composition of the different tephra layers has not incidence on the variance between both instruments. The variance of the SEM relatively to the EPMA is

reported in Table 1. Variance was not calculated for the P_2O_5, which is under the detection limit of the EDS analyses. The intercalibration shows the full comparability of the EPMA-CAMPARIS and SEM-DST. The different tephra layers were classified using the Total Alkali vs. Silica diagram (TAS, Le Bas et al., 1986; Fig. 3).

2.3 Stable isotope analysis

Oxygen isotope measurements were obtained on the planktonic foraminifera *Globigerinoides ruber* (250-315 μm) with a sampling resolution every 10 cm. Between 6 to 10 shells were picked and then cleaned in a methanol ultrasonic bath for few seconds then roasted under vacuum at 380°C for 45 minutes, prior to isotopic analyses. Isotopic composition was expressed in δ-‰ unit and normalized to the Vienna Pee Dee Belemnite scale (V-PDB) using the international standards NBS18. Analyses were performed at the Laboratoire des Sciences du Climat et de l'Environnement (LSCE, Gif-sur-Yvette, France) using a Finnigan Delta Plus mass-spectrometers. The mean external reproducibility (1σ) of carbonate standards (NBS18 $\delta^{18}O$= -23.2 ± 0.1‰) was ± 0.05‰.

2.4 Radiocarbon dating

Radiocarbon analyses were performed by UMS-ARTEMIS (Pelletron 3MV) AMS facilities (CNRS-CEA Saclay, France) on monospecific planktonic foraminifera in the size fraction >150μm (Table 2). To minimize the effect of bioturbation, the sampling was limited to peaks of maximum abundance of planktonic foraminifera (Bard et al., 1987). The conventional radiocarbon ages were subsequently converted into calendar ages, based on INTCAL09 (Reimer et al., 2009) using the ^{14}C calibration software CALIB 6 (Stuiver et al., 1998). The calibration integrate a marine reservoir correction R(t) of about 400 years (Siani et al., 2000).

2.5 Rock magnetic properties

A total of 539 samples were collected at ca. 3 cm interval along the total core length, using plastic cubic boxes of standard size (2 cm of length). Measurements were carried out at the ALP palaeomagnetic laboratory (Peveragno, Italy). Magnetic susceptibility (k), natural remnant magnetization (NRM) and NRM demagnetized in alternating field (AF) at 25 mT peak-field (NRM_{25}) were measured using a KLY-3 kappabridge and a 2G cryogenic magnetometer respectively. After completion of all measurements, the samples were dried and weighted in order to normalize the magnetic parameters by the mass. The mean water content was in the order of 40-50%

3. Results

3.1 Age model

The stratigraphy of core MD 90-918 was derived from the $\delta^{18}O$ variations of the planktic foraminifera *Globigerinoides ruber* (Fig. 2). The $\delta^{18}O$ values range between 3.5 to -0.3 ‰ exhibiting a pattern similar to those observed in nearby south Adriatic deep-sea cores (Fontugne et al., 1989; Siani et al. 2001, 2010). The late glacial, the last glacial/interglacial transition and the Holocene encompass the upper 1470 cm of the core, leading to a highly detailed record of both the two-steps of the deglaciation marked by two abrupt shifts toward depleted $\delta^{18}O$ values from 590 cm to 430 cm and from 300 cm to 230 cm (Termination IA and IB; Duplessy et al., 1981; Bard et al., 1987) and the Holocene.

The age model of the core MD 90-918 was then based on 7 AMS ^{14}C measurements performed on monospecific planktonic foraminifera in the size fraction >150μm (Table 2), by a linear interpolation of two consecutive ages. In addition, comparison of the oxygen isotope

record with that of the South Adriatic Sea core MD 90-917 previously dated by several AMS ^{14}C ages (Siani et al., 2001; 2010) provides three more age control points at 300 cm, 420 cm, and 590 cm. Combination of the age points resulting from the two times series provides a consistent age model covering the last 27.4 cal ka BP (Fig. 2). The calculated sedimentation rate is estimated between 30 cm/ka (from the top to 470 cm depth), for the last glacial/interglacial transition to Holocene section and 92 cm/ka during the late Glacial (Fig. 2).

3.2 Rock-magnetism

Down-core mass susceptibility is shown in Figure 2. Mass susceptibility shows rather uniform values along the core. As a whole, results indicate little fluctuations of the magnetic mineralogy, both in magnetic grain concentration and mineral type. The lower values between 204 to 231 cm depth correspond to the S1 Sapropel interval. Four distinct spikes occur at 73.5, 771, 887 and 982 cm. The 982 cm spike could be correlated to a turbiditic sandy layer, whereas the other three do not match evidences of lithological changes. No one of the tephra layers found in the core match a distinctive change in the magnetic properties. This is probably due to both their small thickness and high content in glass and micropumice. This justify the glass-shard counting procedure used for tephra identification.

3.3 Composition and origin of tephra layers

The geochemical composition and the morphological characteristic of vitric fragments are here presented for determining the proximal counterparts and the origins of the marine tephra layers (Figs. 3 and 4). One tephra and seven cryptotephra layers were recognized along the core MD 90-918 and centred at 2, 175, 185, 210, 218, 223, 230 and 820 cm respectively spanning the last 27.4 cal ka BP (Fig. 2). In particular, tephra layers between 210 and 230 cm

form a cluster with high abundance of volcanic glass-shards (Fig. 4). Only the peak at 223 cm is visible at naked eye inspection, while the other peaks were identified through the high resolution counting of glass shards.

The cryptotephra centred at ***2 cm*** was dated at 0.6 cal ka BP (ca. AD 1335, Table 2) and presents a homogeneous rhyolitic composition (Fig. 3; Table 3). It contains glass shards with a glassy groundmass (Fig. 5a), and mean grain size coarser than 100 μm. The vesicles are elongated to form fibrous glass shards.

The cryptotephra at ***175 cm*** and ***185 cm*** are dated at 7 and 7.3 cal ka BP, respectively (Table 2). Both tephra present a homogeneous Na-phonolitic composition (Fig. 6b; Table 3) and are equally characterised by highly vesicular, aphyric, white micropumices with a grain size finer than 100 μm, and a glassy groundmass (Figs. 5b and c). The only difference concerns the major elements analyses of the tephra at 185 cm showing a double Na-phonolitic composition, with slight differences in CaO, Na_2O, K_2O and SiO_2 contents (Table 3).

The cryptotephra at ***210 cm*** presents a high glass abundance (Fig. 2). Inspection under stereo-microscope shows that ca. 90 % of the volcanic glass are white micropumice and the other 10 % glass shards (Fig. 4). Micropumice fragments are highly vesicular and aphyric, with a glassy groundmass with grain size finer than 100 μm. The second ones are small rounded bubbles and aphyric, glassy groundmass with grain size finer than 50 μm (Fig. 5d). The composition of micropumice fragments is homogeneous Na-phonolitic (Fig. 6b; Table 3), very similar to the cryptotephra at 175 and 185 cm and present an interpolated age at ca. 8.1 cal ka BP. On the other hand, few glass shards show a homogeneous rhyolitic composition (Fig. 6c; Table 3) representing the tails of the following tephra layer centred at ***218 cm*** (Fig. 4). This crytotephra spreads between 216 and 219 cm and was deposited during the Sapropel S1 interruption. It presents a homogeneous rhyolitic composition and an age of 8.3 cal ka BP

(Fig. 6c; Tables 2 and 3). This cryptotephra contains aphyric glass shards with small rounded bubbles and a mean grain size finer than 50 μm (Fig. 5e).

The tephra layer at ***223 cm*** is visible at naked eye, and contains exclusively highly-vesicular micro-pumices with rounded bubbles and a glassy groundmass (Fig. 5f). The glass composition is Na-phonolitic (K_2O/ Na_2O lower than 1) with high Al_2O_3 content (Fig. 6b; Table 3), and is similar to those of the cryptotephra at 175, 185 and 210 cm. The interpolated age is of ca. 8.6 cal ka BP.

The cryptotephra at ***230 cm*** comprises white, aphyric and highly vesicular micro-pumice with a glassy groundmass and a mean grain size around 50 μm (Fig. 5g). The glass-shards have a Na-phonolitic composition, with high Al_2O_3 content (Fig. 6b; Table 3), and is similar to the previous cryptotephra at 175, 185, 210 and 223 cm. Calibrated radiocarbon dating for this tephra layer gives an age of 9 cal ka BP (Table 2).

The last cryptotephra was recovered at ***820 cm*** and dated at 19.4 cal ka BP (Table 2). It is composed of glass shards coarser than 100 μm (Fig. 5h) with a glassy groundmass and rounded bubbles. The composition straddles between the trachytic and the rhyolitic fields (Fig. 6d; Table 3).

4. Discussion

The available AMS ^{14}C ages and oxygen isotope stratigraphy indicate that the deep-sea core MD 90-918 covers the late Pleistocene to Holocene period (i.e. the last 27.4 cal ka BP). This constrains the search for the source of the parent eruptions of marine cryptotephra and tephra layers to the explosive activity of Mediterranean volcanoes during this time interval.

The recognized cryptotephra and tephra layers show alkaline and calc-alkaline affinity (Fig. 3). The alkaline samples have mildly undersaturated glass compositions with alkali ratio around or below 1 (Na-phonolites; Fig. 3; Table 3), and are younger than 9 ka (Fig. 2). The composition and geochemical affinity limit their sources to Italian volcanoes, since the sources in the Aegean area during the Holocene present a calc-alkaline affinity (e.g. Keller et al., 1978). Sources from Massif Central (France) and Anatolia (Turkey, eastern Mediterranean) can be rejected, though both volcanisms present K-alkaline affinity (Juvigné, 1987; Druitt et al., 1995), because their relatively low dispersion for the former and the upwind location of the study core with respect to the Anatolian volcanoes (e.g. Zanchetta et al., 2011).

The only Holocene source of K-alkaline, undersaturated magmas in the Mediterranean area is Somma-Vesuvius (Santacroce et al., 2008), representing the inferred source for cryptotephra at 175, 185, 210, 230 cm and the tephra layer at 223 cm. The geochemistry of Holocene explosive products of Somma-Vesuvius (Santacroce et al., 2008*)* shows that Na-phonolitic magmas fed the eruptions of the Pomici di Mercato (Santacroce, 1987; Aulinas et al., 2008; Mele et al., 2010), and the initial stages of the Pomici di Avellino (ca. 3.8 ka BP, Sulpizio et al., 2008, 2010). Because the Pomici di Mercato and the Pomici di Avellino (white pumice) products show very different crystal content (almost aphyric vs. porphyritic; Aulinas et al., 2008; Santacroce et al., 2008; Mele et al., 2010; Sulpizio et al., 2010), the glassy, aphyric, Na-phonolitic micropumice and glass shards of the MD 90-918 core can be confidently correlated to the Pomici di Mercato eruption (ca. 8.5 cal ka BP; Zanchetta et al., 2011).

Nevertheless, the attribution to the Pomici di Mercato eruption poses some problems in layer by layer correlation of the Na-phonolitic cryptotephra and tephra layer to the proximal stratigraphy of Somma-Vesuvius. The tephrostratigraphy of core MD 90-918 indicates 5 distinct depositional events over a time span of ca. 2000 years. On the basis of this

chronology, the correlation to a single eruption is unlikely, although the Mercato eruption was recently described as a long lasting, pulsating event (Mele et al., 2010). Based on field evidences, a reasonable duration of the Mercato eruption can be assessed at some decades at maximum, but in any case neither to centuries nor to millennia.

The chronology of the Pomici di Mercato eruption spans from a maximum age of 9010 ± 130 cal yr BP (Wulf et al., 2004) to 8540 ± 50 cal yr BP (Zanchetta et al., 2011). These ages are in fairly good agreement with that reported in Delibrias et al. (1979), which provided a calibrated age at ca. 9.1 cal ka BP (paleosoil under the Pomici di Mercato deposits, PSV 112 and PSV 113 samples), although ages obtained with ^{14}C method before 1980 needs to be considered with caution (Santacroce et al., 2008). This age range is in agreement with dating of both ***230 cm*** cryptotephra (8470 ± 50 cal yr BP) and ***223 cm*** tephra (interpolated age of 8.6 cal ka BP) layers, making it difficult to precisely individuate the onset of the Pomici di Mercato eruption in core MD 90-918. In particular, it is difficult to discriminate if the cryptotephra at 230 cm represents the first eruptive phase of the Pomici di Mercato eruption or a small event preceding the main eruption and not known in proximal areas, since the deposits between the Greenish and Mercato eruptions (e.g. Santacroce et al., 2008) have homogeneous K-trachytic composition (e.g. GM1; Zanchetta et al., 2000; Siani et al., 2004).

The cryptotephra at ***210 cm*** is about 500 years younger (interpolated age of 8.1 ka) than the tephra layer at 223 cm. Because it occurs within few centuries from the preceding tephra layer, a correlation to the latest stages of the Mercato eruption is still possible. In particular, it may be correlated to the Phase III of the eruption (Mele et al., 2010; previously known as Pomici and Proietti; Santacroce, 1987), which is separated by the preceding Phase II by erosion surfaces indicating volcanic quiescence between them.

A distinct discussion requires the origin of the cryptotephra at ***175 and 185 cm***. Their radiocarbon ages are significantly younger (between 7 and 7.3 cal ka BP) than the proximal

Pomici di Mercato deposits (8.5 cal ka BP), so their correlation to this eruption still remains problematic. Firstly, stratigraphy, sedimentology, rock magnetic data and chronology of the core exclude extensive reworking of the sediment core (i.e. presence of sand layers indicative of turbidite deposits, large bioturbation, etc.). On the other hand, the two cryptotephra at 175 and 185 cm do not correspond to a distal counter part of known activity between the eruptions of Mercato and Avellino, of the well known and detailed Somma-Vesuvius stratigraphy (e.g. Santacroce and Sbrana, 2003; Cioni et al., 2008; Santacroce et al., 2008). However, tephrostratigraphy study from Holocene lake sediments of the Sulmona basin indicates the occurrence of numerous tephra layers, occurred between Pomici di Mercato and Avellino eruptions, which have not correlations with proximal deposits of Italian volcanoes (Giaccio et al., 2009). Nevertheless, the occurrence of subplinian events between Pomici di Mercato and Avellino eruption was reproted by Delibrias et al., (1979) and chronologically constrained between two paleosoils dated at 8.6 and 6.3 cal ka BP (Alessio et al., 1974; Delibrias et al., 1979). The origin of these Mercato-Avellino cryptotephra (MA group) remains enigmatic, and we cannot rule out they could represent distal evidence of unknown Vesuvian activity.

Tephra layers compositionally similar to the Pomici di Mercato deposits were found in lacustrine (TM6b in the Lago Grande di Monticchio; Wulf et al., 2004, 2008; OT02-3 in Lake Ohrid; Vogel et al., 2010), and marine (KET 8218, Adriatic Sea; Paterne et al., 1988) cores (Table 4). The recognition in core MD 90-918 enlarges the dispersal ash area of the Mercato products to the southeast with an estimated geographical distribution at ca. 250,000 km² (Fig. 7).

Homogeneous rhyolitic cryptotephra with calc-alkaline affinity occur between ***2 and 5 cm*** and between ***216 and 219 cm***. The available ^{14}C age measurements constrain the former interval at ca. 0.6 cal ka BP, and the latter at ca 8.3 cal ka BP (Table 2). During this period,

calc-alkaline tephra were generated by explosive activity of both Aegean arc (Greece, eastern Mediterranean) and Aeolian Islands volcanoes (southern Tyrrhenian Sea, central Mediterranean). The evolved magmas from these two sources are hardly distinguishable considering major and trace elements (Clift and Blusztajn, 1999). However, a source in the Aegean Sea is unlikely taking into account the prevailing winds in the area, which preferentially blow from west to east (Barberi et al., 1990; Costa et al., 2009; Folch and Sulpizio, 2010). Therefore, an Aeolian Island origin is here assumed.

The rhyolitic tephra layer at the top of the core (***2-5 cm***; Fig. 2) is dated at ca. 0.6 cal ka BP (AD 1321 – 1349; Table 2). Age and composition suggest a correlation to the eruption of Monte Pilato from Lipari Island (Fig. 6a; Table 4), recently dated by archaeomagnetic techniques between AD 1030-1528 (Zanella, 2006) or AD 1200-1240 (Arrighi et al., 2006). This is the first recognition of Monte Pilato tephra in deep-sea cores of the Ionian Sea, and enlarges the dispersal of this tephra to the East (Fig. 7).

The composition and the stratigraphy of the cryptotephra between ***216 and 219 cm*** matches well that of the rhyolitic tephra layer E-1 (Paterne et al., 1988; Fontugne et al., 1989; Fig. 6c; Table 4), which is correlated to the eruption of Gabellotto-Fiumebianco from Lipari Island (Siani et al., 2004; Zanchetta et al., 2010). Siani et al. (2004) dated this eruption at 8.4 cal ka BP through ^{14}C AMS measurements on planktic foraminifera, an age in good agreement with that of the 216-219 cryptotephra in core MD 90-918, dated at 8.3 cal ka BP. The recognition of Gabellotto-Fiumebianco/E-1 tephra layers in core MD 90-918 enlarges its dispersal area to the east (Fig. 7). The surface of the dispersal ash area can now be estimated at ca. 300,000 km². Moreover, it is interesting to point out that E-1 tephra recovered in cores MD 90-918 and MD 90-917 presents a similar stratigraphic position between the end of the Sapropel S1a interval and the Sapropel interruption.

The cryptotephra at ***820 cm*** is trachy-rhyolitic in composition, and is dated at 19.4 cal ka BP (Table 2). These findings allow to correlate this tephra to the eruption of Monte Guardia from Lipari Island. This is mainly because, among the known eruptions with trachy-rhyolitic composition occurred around 20 cal ka BP like those of the Lower Pollara (Salina Island, 24 cal ka BP; Calanchi et al., 1993), the Lentia cycle (Vulcano Island, 15-25 cal ka BP; De Astis et al., 1997), and the third and fourth cycles from Pantelleria Island (Civetta et al., 1988), it shows the best geochemical match (Fig. 6d; Table 4). In particular, the ***820 cm*** tephra can be correlated to the less evolved component of the Monte Guardia eruption (MG4 base B sample; Table 4), which is characterised by an important geochemical variability due to pre- and sin-eruptive processes of magma mixing and mingling (De Rosa et al., 2003). The Monte Guardia eruption from Lipari Island has an age comprised between 22.4 ± 1.1 cal ka BP and 20.3 ± 0.7 cal ka BP (Crisci et al., 1981, 1991; De Rosa and Sheridan, 1983), which is in fairly good agreement with that obtained for the cryptotephra at 820 cm.

The evolved products of the Monte Guardia eruption were also recognized in the sediments of the Lago di Pergusa (central Sicily; Fig. 1; Narcisi, 2002), and this suggest different dispersal areas for ash produced at different times during the eruption. The first time recognition of Monte Guardia tephra in the Ionian Sea sediments enlarges the dispersal area to the East (Fig. 7).

5. Concluding remarks

Seven cryptotephra and one tephra layer were identified in core MD 90-918: five of them are from Somma-Vesuvius and three from Lipari Island (Aeolian archipelago).

Tephra layers from Somma-Vesuvius are compositionally homogeneous Na-phonolites, and are correlated to the Mercato eruption. Among them, only the tephra layer at 223 cm and the cryptotephra at 210 cm are related to primary tephra deposition from a pyroclastic cloud, while the depositional processes of the other three still remain puzzling. In particular, the two upper Na-phonolitic cryptotephra are too young to be correlated to the Mercato eruption. They may represent an interplinian activity occurred between the Mercato and Avellino Plinian eruptions (MA group), though proximal counterparts are not described in the well known Somma-Vesuvius stratigraphy. However, new tephrochronology studies from distal archives are needed to confirm the presence of this activity. The tephra layer at 223 cm occurs within the Sapropel S1, confirming the Mercato eruption as a good marker for the Sapropel S1a interval.

Cryptotephra from Lipari Island are all rhyolitic, and are correlated to Monte Pilato (2 cm, AD 1030-1528), Gabellotto-Fiumebianco (E-1, 218 cm, 8.4 cal ka BP), and Monte Guardia (820 cm, between 22.4 ± 1.1 cal ka BP and 20.3 ± 0.7 cal ka BP). Two of them (Monte Pilato and Monte Guardia) are for the first time recognized in the marine sediments of the Ionian Sea, and enlarges significantly the dispersion of these tephra to the East.

Acknowledgements

We thank the Centre National de la Recherche Scientifique (CNRS) and Commissariat à l'Energie Atomique (CEA) for basic support to the laboratory. We also thank the N/O Marion Dufresne officers and crew for support and organisation of the coring cruises. BC was partially supported by Vinci program of Université Franco-Italienne and SETCI from region of Île-de-France. Elisabeth Michel (LSCE), Franco Colarieti (DST Pisa), Michel Fialin and Frederic Couffignal (CAMPARIS) are gratefully acknowledged for the preparation of samples and assistance during analyses. Partial funding support comes from University of

Pisa (Fondi di Ateneo R. Santacroce, G. Zanchetta), INGV-DPC projects (Leader R. Santacroce), and SPEED-INGV project. RS acknowledge partial funding from IUGG grants 2010-2011.

References

Alessio, M., Bella, F., Improta, S., Belluomini, G., Calderoni, G., Cortesi, C., Turi, F., 1974. University of Rome carbon-14 dates X. *Radiocarbon*, 16: 358-367.

Arrighi, S., Tanguy, J.C., Rosi, M., 2006. Eruptions of the last 2200 years at Vulcano and Vulcanello (Aeolian Islands, Italy) dated by high-accuracy archeomagnetism. *Physics of the Earth and Planetary Interiors*, 159, 225–233. doi:10.1016/j.pepi.2006.07.010.

Aulinas, M., Civetta, L., Di Vito M.A., Orsi, G., Gimeno, D., Fèrnandes-Turiel, J.L., 2008. The "pomici di mercato" Plinian eruption of Somma-Vesuvius: magma chamber processes and eruption dynamics. *Bulletin of Volcanology*, 70, 825-840.

Barberi, F., Macedonio, G., Pareschi, M.T., Santacroce, R., 1990. Mapping the tephra fallout risk: an example from Vesuvius, Italy. *Nature*, 344, 142-144.

Bard, E., Arnold, M., Duprat, J., Moyes, J., Duplessy, J.C., 1987. Reconstruction of the last deglaciation: deconvolved records of $\delta^{18}O$ profiles, micropaleontological variations and accelerator mass spectrometric ^{14}C dating. *Climate Dynamics*, 1, 101-112.

Bourne, A.J., Lowe, J.J., Trincardi, F., Asioli, A., Blockley, S.P.E., Wulf, S., Matthews, I.P., Piva, A., Vigliotti, L., 2010. Distal tephra record for the last ca 105,000 years from core PRAD 1-2 in the central Adriatic Sea: implications for marine tephrostratigraphy. *Quaternary Science Reviews*, 29 : 3079-3094.

Calanchi, N., De Rosa, R., Mazzuoli, R., Rossi, P., Santacroce, R., Ventura, G., 1993. Silicic magma entering a basaltic magma chamber: eruptive dynamics and magma mixing – an example from Salina (Aeolian Islands, Southern Tyrrhenian Sea). *Bulletin of Volcanology*, 55, 504-522.

Cioni, R., Bertagnini A., Santacroce, R., Andronico, D., 2008. Explosive activity and eruption scenarios at Somma-Vesuvius (Italy): towards a new classification scheme. *Journal of Volcanology and Geothermal Research*, 178, 331-348.

Civetta, L., Cornette, Y., Gillot, P.Y., Orsi, G., 1988. The eruptive history of Pantelleria (Sicily Channel) in the last 50 ka. *Bulletin of Volcanology*, 50, 47-57.

Clift, P., Blusztajn, J., 1999. The trace-element characteristics of Aegean volcanic arc marine tephra. *Journal of Volcanology and Geothermal Research*, 92, 321-347.

Costa, A., Dell'Erba, F., Di Vito, M.A., Isaia, R., Macedonio, G., Orsi, G., Pfeiffer, T., 2009. Tephra fallout hazard at the Campi Flegrei caldera (Italy). *Bulletin of Volcanology*, 71, 259-273.

Crisci, G.M., De Rosa, R., Lanzafame, G., Mazzuoli, R., Sheridan, M.F., Zuffa, G.G., 1981. Monte Guardia sequence: a late-Pleistocene eruptive cycle on Lipari. *Bulletin of Volcanology*, 44, 241–255.

Crisci, G.M., De Rosa, R., Esperanca, S., Mazzuoli, R., Sonnino, M., 1991. Temporal evolution of a three component system: the island of Lipari (Aeolian Arc, southern Italy). *Bulletin of Volcanology*, 53, 207–221.

De Astis, G., La Volpe, L., Peccerillo, A., Civetta, L., 1997. Volcanological and petrological evolution of Vulcano Island (Aeolian Arc, southern Tyrrhenian Sea). *Journal of Geophysical Research*, 102, 8021-8050.

De Rosa, R., Sheridan, M.F., 1983. Evidence for magma mixing in the surge deposits of the Monte Guardia Sequence, Lipari. *Journal Volcanology Geothermal Research*, 17, 313–328.

De Rosa, R., Donato, P., Gioncada, A., Masetti, M., Santacroce, R., 2003. The Monte Guardia eruption (Lipari, Aeolian Islands): an unusual example of magma mixing sequence. B*ulletin of Volcanology*, 65, 530–543.

Delibrias, G., Di Paola, G.M., Rosi, M., Santacroce, R.,1979. La storia eruttiva del complesso vulcanico Somma-Vesuvio ricostruita dalle successioni piroclastiche del Monte Somma. *Rendiconti della Societa Italiana di Mineralogia e Petrologia*, 35: 411-438.

Druitt, T.H., Brenchley, P.J., Gökten, Y.E., Francaviglia, V., 1995. Late Quaternary rhyolitic eruption from the Acigöl Complex, central Turkey. *Journal of Geological Society of London*, 152, 655–667.

Duplessy, J.C., Delibrias, G., Turon, J.L., Pujol, C., Duprat, J., 1981. Deglacial warming of the northeastern Atlantic ocean: correlation with paleoclimatic evolution of the European continent. *Palaeogeography, Palaeoclimatology, Palaeoecology*, 35, 121-144.

Folch, A., Sulpizio, R., 2010. Evaluating the long-range volcanic ash hazard using supercomputing facilities. Application to Somma-Vesuvius (Italy), and consequences on civil aviation over the Central Mediterranean Area. *Bulletin of Volcanology*, doi: 10.007/s0045-010-03863.

Fontugne, M., Paterne, M., Calvert, S., Murat, A., Guichard, F., Arnold, M., 1989. Adriatic deep water formation during the Holocene: implication for the reoxygenation of the deep eastern Mediterranean sea. *Paleoceanography*, 4, 199-206.

Giaccio, B., Messina, P., Sposato, A., Voltaggio, M., Zanchetta, G., Galadini, F., Gori, S., Santacroce, R., 2009. Tephra layers from Holocene lake sediments of the Sulmona Basin, central Italy: implications for volcanic activity in Peninsular Italy and tephrostratigraphy in the central Mediterranean area. *Quaternary Science Review*, 28 : 2710-2733.

Juvigné, E., 1987. Deux retombées volcaniques tardiglaciaires dans le cézallier (Massif Central, France). *Bulletin de l'Association Française pour l'étude du Quaternaire*, 4, 241-249.

Kallel, N., Paterne, M., Labeyrie, L., Duplessy, J.C., Arnold, M., 1997. Temperature and salinity records of the Tyrrhenian Sea during the last 18,000 years. *Palaeogeography, Palaeoclimatology, Palaeoecology*, 135, 97-108.

Keller, J., Ryan, W.B.F., Ninkovich, D., Altherr, R., 1978. Explosive volcanic activity in the Mediterranean over the past 200,000 yr as recorded in deep-sea sediments. *Geological Society American Bulletin*, 89, 591–604.

Lane, C.S., Blockley, S.P.E., Lotter, A.F., Fisinger, W., Filippi, M.L. and Matthews, I.P. (2010). A regional tephrostratigraphic framework for central and southern European climate archives during the Last Glacial to Interglacial Transition: comparisons north and south of the Alps. *Quaternary Science Reviews* (in press) doi:10.1016/j.quascirev.2010.10.015.

Le Bas, M.J., Le Maitre, R.W., Streckeisen, A., Zanettin, B., 1986. A chemical classification of volcanic rocks based on the total alkali-silica diagram. *Journal of Petrology*, 27, 745–750.

Lowe, J.J., Blockley, S., Trincardi, F., Asioli, A., Cattaneo, A., Matthews, I.P., Pollard, M., Wulf, S., 2007. Age modelling of late Quaternary marine sequences in the Adriatic: towards improved precision and accuracy using volcanic event stratigraphy. *Continental Shelf Research*, 27, 560–582.

Margari, V., Pyle, D.M, Brynt, C., Gibbart, P.L., 2007. Mediterranean tephrostratigraphy revisited: results from a long terrestrial sequence on Lesvos Island, Greece. *Journal of Volcanology and Geothermal Research*, 163, 34-54.

McCoy, F.W. 1981. Areal distribution, redeposition and mixing of tephra within deep-sea sediments of the Eastern Mediterranean Sea. *In Self, S and Sparks, RSJ (Editors), Tephra Studies. Reidel Dordrecht*, 245-254.

Mele D., Sulpizio R., Dellino P., La Volpe L., (2010). Stratigraphy and eruptive dynamics of a long-lasting Plinian eruption of Somma-Vesuvius: the Pomici di Mercato (8900 years BP). *Bulletin of Volcanology*, doi 10.007/S00445-010-0407-2.

Mercone, D., Thomson, J., Croudace, I.W., Siani, G., Paterne, M., Tröelstra, S., 2000. Duration of S1, the most recent Eastern Mediterranean sapropel, as indicated by AMS radiocarbon and geochemical evidence. *Paleoceanography*, 15, 336-347.

Narcisi, B., 2002. Tephrostratigraphy of the Late Quaternary lacustrine sediments of Lago di Pergusa (central Sicily). *Bollettino Società Geologica Italiana*, 121, 211-219.

Paterne, M., Guichard, F., Labeyrie, J., Gillot, P.Y., Duplessy, J.C., 1986. Tyrrhenian Sea tephrochronology of the oxygen isotope record for the past 60,000 years. *Marine Geology*, 72, 259-285.

Paterne, M., Guichard, F., Labeyrie, J., 1988. Explosive activity of the South Italian volcanoes during the past 80,000 years as determined by marine tephrochronology. *Journal of Volcanology Geothermal Research*, 34, 153-172.

Paterne, M., Labeyrie, J., Guichard, F., Massaud, A., Maitre, F., 1990. Fluctuation of the campanian explosive activity (South Italy) during the last 190,000 years as determined by marine tephrochronology. *Earth and Planetary Science Letters*, 98, 166-174.

Paterne, M., Guichard, F., Duplessy, J.C., Siani, G., Sul pizio, R., Labeyrie, J., 2008. A 90,000 – 200,000 yrs marine tephra record of Italian volcanic activity in the central Mediterranean Sea. *Journal of Volcanology and Geothermal Research*, 177, 187–196.

Reimer, P.J., Baillie, M.G.L., Bard, E., Bayliss, A., Beck, J.W., Blackwell, P.G., Bronk Ramsey , C., Buck, C.E., Burr, G.S., Edwards, R.L., Friedrich, M., Grootes, P.M., Guilderson, T.P., Hajdas, I., Heaton, T.J., Hogg, A.G., Hughen, K.A., Kaiser, K.F., Kromer, B., McCormac, F.G., Manning, S.W., Reimer, R.W., Richards, D.A., Southon, J.R., Talamo, S., Turney, C.S.M., van der Plicht, J. and Weyhenmeyer, C.E. (2009) INTCAL 09 and MARINE09 radiocarbon age calibration curves, 0-50,000 years Cal BP. *Radiocarbon*, 51: 1111-1150. ISSN 0033-8222.

Rohling, E.J., Jorissen, F.J., De Stigter, H.C., 1997. 200 year interruption of Holocene sapropel formation in the Adriatic sea. *Journal of Micropaleontolology*, 16, 97-108.

Santacroce, R., (ed.) 1987. Somma-Vesuvius. *Quaderni la Ricerca, Scietifica*, 114, 200 pp.

Santacroce, R. and Sbrana, A., 2003. Geological map of Somma-Vesuvius, scale 1:15000. *Selca, Firenze*.

Santacroce, R., Cioni, R., Marianelli, P., Sbrana, A., Sul pizio, R., Zanchetta, G., Donahue, D.J., Joron, J.L., 2008. Age and whole rock-glass compositions of proximal pyroclastics from

the major explosive eruptions of Somma-Vesuvius: a review as a tool for distal tephrostratigraphy. *Journal of Volcanology and Geothermal Research*, 177, 1–18.

Siani, G., Paterne, M., Arnold, M., Bard, E., Métivier, B., Tisnerat, N., Bassinot, F., 2000. Radiocarbon reservoir ages in the Mediterranean Sea and Black Sea coastal waters. *Radiocarbon*, 42 (2), 271–280.

Siani, G., Paterne, M., Michel, E., Sulpizio, R., Sbrana, A., Arnold, M., Haddad, G., 2001. Mediterranean sea-surface radiocarbon reservoir age changes since the last glacial maximum. *Science*, 294, 1917-1920.

Siani, G., Sulpizio, R., Paterne, M., Sbrana, A., 2004. Tephrostratigraphy study for the last 18,000 14C years in a deep-sea sediment sequence for the South Adriatic. *Quaternary Science Review*, 23, 2485-2500.

Siani G., Paterne, M., Colin, C. (2010) - Late Glacial to Holocene planktic foraminifera bioevents and climatic record in the South Adriatic Sea. *Journal of Quaternary Science*, 25: 808-821.

Stuiver, M., Reimer, P.J., Bard, E., Beck, J.W., Burr, G.S., Hughen, K.A., Kromer, B., McCormac, G., van der Plicht, J., Spurk, M., 1998. INTCAL98 radiocarbon age calibration, 24000-0 cal BP. *Radiocarbon*, 40, 1041–1083.

Sulpizio, R., Bonasia, L., Dellino, P., La Volpe, P., Mele, Zanchetta, G., Di Vito, M.A., Sadori, L., 2008. Discriminating the long distance dispersal of fine ash from sustained columns or near ground ash clouds: the example of the Avellino eruption (Somma-Vesuvius, Italy). *Journal of Volcanology and Geothermal Research*, 177, 263-276.

Sulpizio, R., Cioni, R., Di Vito, M.A., Mele, D., Bonasia, R., Dellino, P., 2010. The Pomici di Avellino eruption of Somma-Vesuvius (3.9 ka BP) part I: stratigraphy, compositional variability and eruptive dynamics. *Bulletin of Volcanology*, in press.

Thunell, R., Federman, A., Sparks, S., Williams, D., 1979. The age, origin, and volcanological significance of the Y-5 ash layer in the Mediterranean. *Quaternary Research*, 12, 241-253.

Turney, C.S.M., Blockley, S.P.E., Lowe, J.J., Wulf, S., Branch, N.P., Mastrolorenzo, G., Swindle, G., Nathan, R., Pollard, A.M., 2008. Geochemical characterization of Quaternary tephras from the Campanian province. Italy. *Quaternary International*, 178, 288–305.

Vogel, H., Zanchetta, G., Sulpizio, R., Wagner, B., Nowaczyk, N., 2010. A tephrostratigraphic record for the last glacial-interglacial cycle from Lake Ohrid, Albania and Macedonia. *Journal of Quaternary Science*, 25, 320-338.

Wulf, S., Kraml, M., Brauer, A., Keller, J., Negendank, J.F.W., 2004. Tephrochronology of the 100 ka lacustrine sediment record of Lago Grande di Monticchio (southern Italy). *Quaternary International*, 122, 7–30.

Wulf, S., Kraml, M., Keller, J., 2008. Towards a detailed distal tephrostratigraphy in the Central Mediterranean: the last 20,000 yrs record of Lago Grande di Monticchio. *Journal of Volcanology and Geothermal Research*, 177, 118–132.

Zanchetta, G., Di Vito, M., Fallick, A.E., Sulpizio, R., 2000. Stable isotopes of pedogenic carbonate from Somma-Vesuvius area, southern italy, over the last 18 ka: palaeoclimatic implications. *Journal of Quaternary Science*, 15 (8), 813-824.

Zanchetta, G., Sulpizio, R., Roberts, N., Cioni, R., Eastwood, W.J., Siani, G., Caron, B., Paterne, M., Santacroce, R., 2011. Tephrostratigraphy, chronology and climatic events of the Mediterranean basin during the Holocene: an overview. *The Holocene*, 21: 33-52, doi: 10.1177/09596683610377531.

Zanella, E., 2006. Magnetic chronology in recent volcanic rocks: basic principles and case histories from Aeolian Islands. *Acta Vulcanologica*, 18 (1-2), 35-46.

Figure and Table captions

Figure 1: Location map of the study area, of the main Italian volcanoes and location of cores used in this study. Legend: CVZ = Campanian Volcanic Zone (Campi Flegrei, Somma-Vesuvius, Ischia and Procida), AI = Aeolian Islands, LGM = Lago Grande di Monticchio, LdP = Lago di Pergusa.

Figure 2: Lithostratigraphy, AMS ^{14}C dates samples location, variations in $\delta^{18}O$ (per mil) of *Globigerina bulloides*, glass shards abundance curve, mass magnetic susceptibility and age model of the deep sea core MD 90-918.

Figure 3: General TAS diagram with geochemical compositions of the marine tephra layers from core MD 90-918 (Le Bas et al., 1986).

Figure 4: Stratigraphy details of the relative abundance and composition of glass shards during the Sapropel S1 in core MD 90-918.

Figure 5: SEM pictures of volcanic glass fragments from tephra layer a) 2 cm, b) 175 cm, c) 185 cm, d) 210 cm, e) 218 cm, f) 223 cm, g) 230 cm and h) 820 cm.

Figure 6: Comparison of the geochemical compositions of the ash-layers in core MD 90-918 with those on the continental and marine deposits from the literature plotted in TAS diagram: a) Monte Pilato eruption ca. AD 1200, samples PI 134 from Lipari Island and correlation with the tephra layer at 2-5 cm; c) Mercato eruption samples from the Somma-Vesuvius (Wulf et al., 2004; Santacroce et al., 2008; Turney et al., 2008 and Paterne et al., 1988) and correlation with the tephra layers at 230, 223, 210, 185 and 175 cm; d) Gabellotto-Fiumebianco eruption and E-1 tephra layer samples from the Lipari Island (Siani et al., 2004; Paterne et al., 1988) and correlation with the tephra layer at 218 cm; e) Monte Guardia eruption samples from the Lipari Island (De Rosa et al., 2003) and correlation with the tephra layers at 820 cm.

Figure 7: Map of the ash dispersion for a) Monte Pilato ca. AD 1200 from Lipari Island, b) Mercato eruption from the Somma-Vesuvius, c) Gabellotto-Fiumebianco eruption from Lipari Island and d) Monte Guardia eruption from Lipari. Stars indicate the volcanic sources.

Table 1: Intercalibration data between SEM-DST (University of Pisa, Italy) and the EPMA-CAMPARIS (University of Pierre et Marie Curie of Paris, France). A set of 99 analyses of five distinct tephra layers is resumed here with: 1) the mean of all analyses from the two instruments; 2) the mean of the analyses from the both instrument; 3) the difference between the means of the analyses from the two instruments; 4) the standard deviation of the means of the analyses from the two instruments; 5) the variance in % of the means of analyses from the two instruments; 6) and finally the average of variance of the distinct layers.

Table 2: Conventional ^{14}C ages from MD 90-918 core determined by UMS-ARTEMIS (Pelletron 3MV) AMS facilities (CNRS-CEA Gif-sur-Yvette, France). The conventional radiocarbon ages were converted into calendar ages, based on INTCAL09 (Reimer et al., 2009) using the ^{14}C calibration software CALIB 6 (Stuiver et al., 1998). The calibration integrate a marine reservoir correction R(t) of about 400 years (Siani et al., 2000).

Table 3: Composition of major elements analyses of the eight tephra layers recognized in core MD 90-918. Analyses performed on the SEM-DST (University of Pisa, Italy) and the EPMA-CAMPARIS (University of Pierre et Marie Curie of Paris, France).

Table 4: Average and standard deviation of analyses from literature used for comparison except the analyses from PI-134 which is a sample collected on the cone Monte Pilato eruptive succession from the Lipari Island.

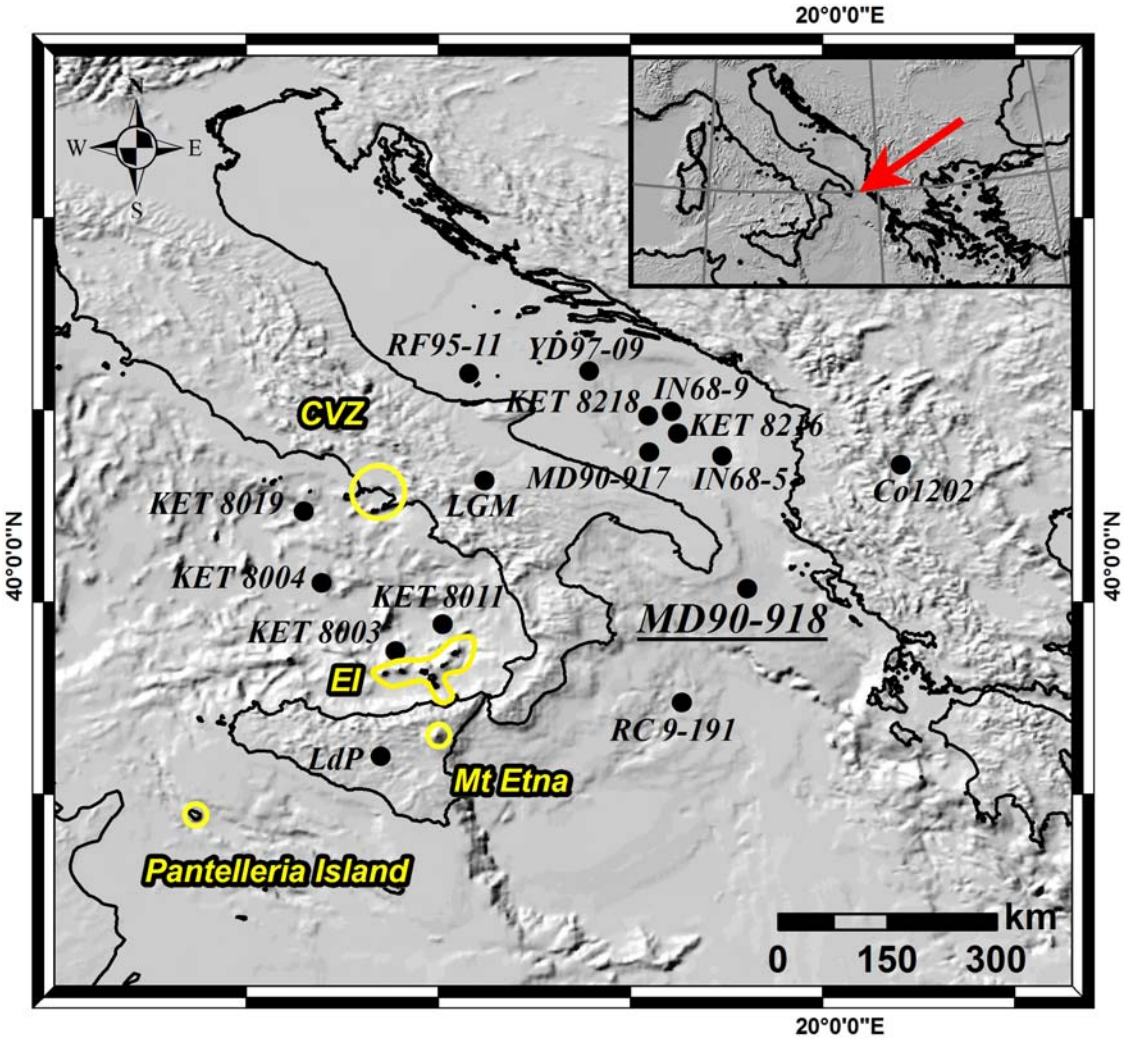
20°0'0"E
N
W
E
S
RF95-11
YD97-09
KET 8218
IN68-9
KET 8216
CVZ
MD90-917
IN68-5
Co1202
KET 8019
LGM
KET 8004
KET 8011
KET 8003
MD90-918
EI
RC 9-191
LdP
Mt Etna
Pantelleria Island
40°0'0"N
km
0
150
300
20°0'0"E

Fig.1

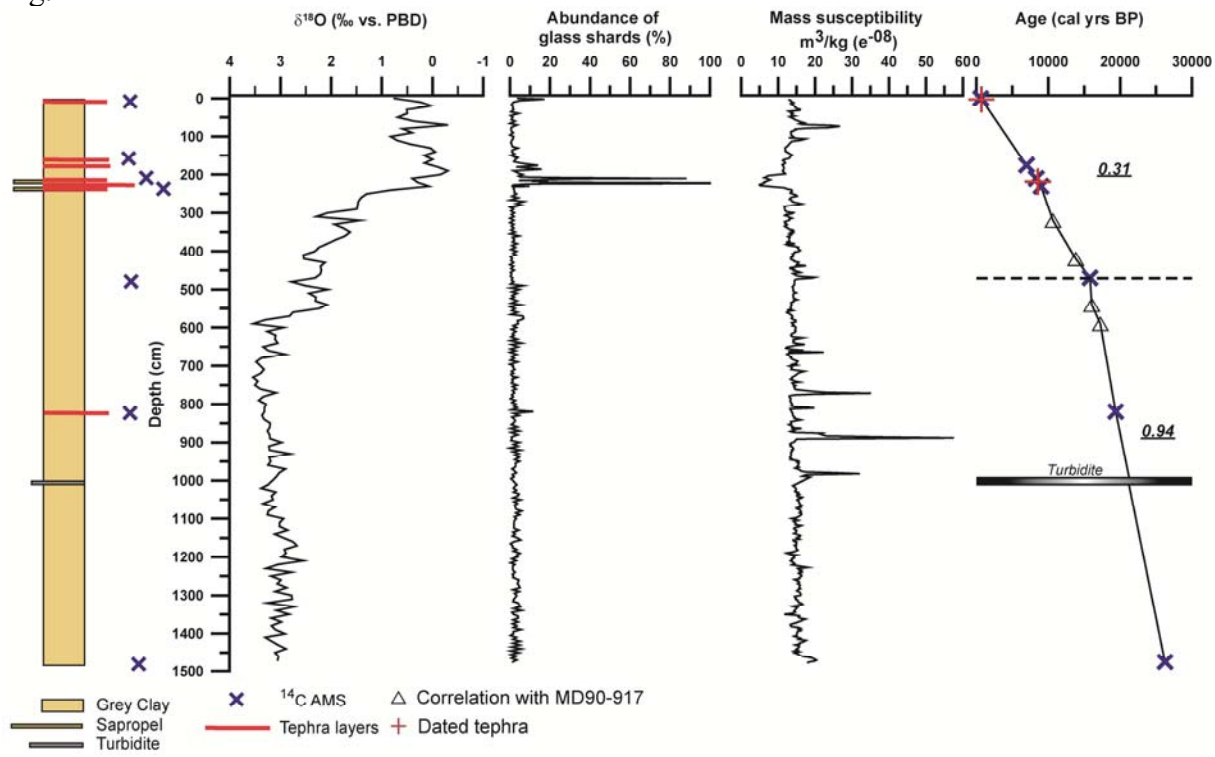
δ18O (‰ vs. PBD)
Abundance of glass shards (%)
Mass susceptibility m3/kg (e-08)
Age (cal yrs BP)
Depth (cm)
0.31
0.94
Turbidite
Grey Clay
Sapropel
Turbidite
14C AMS
Tephra layers
Correlation with MD90-917
Dated tephra

Fig.2

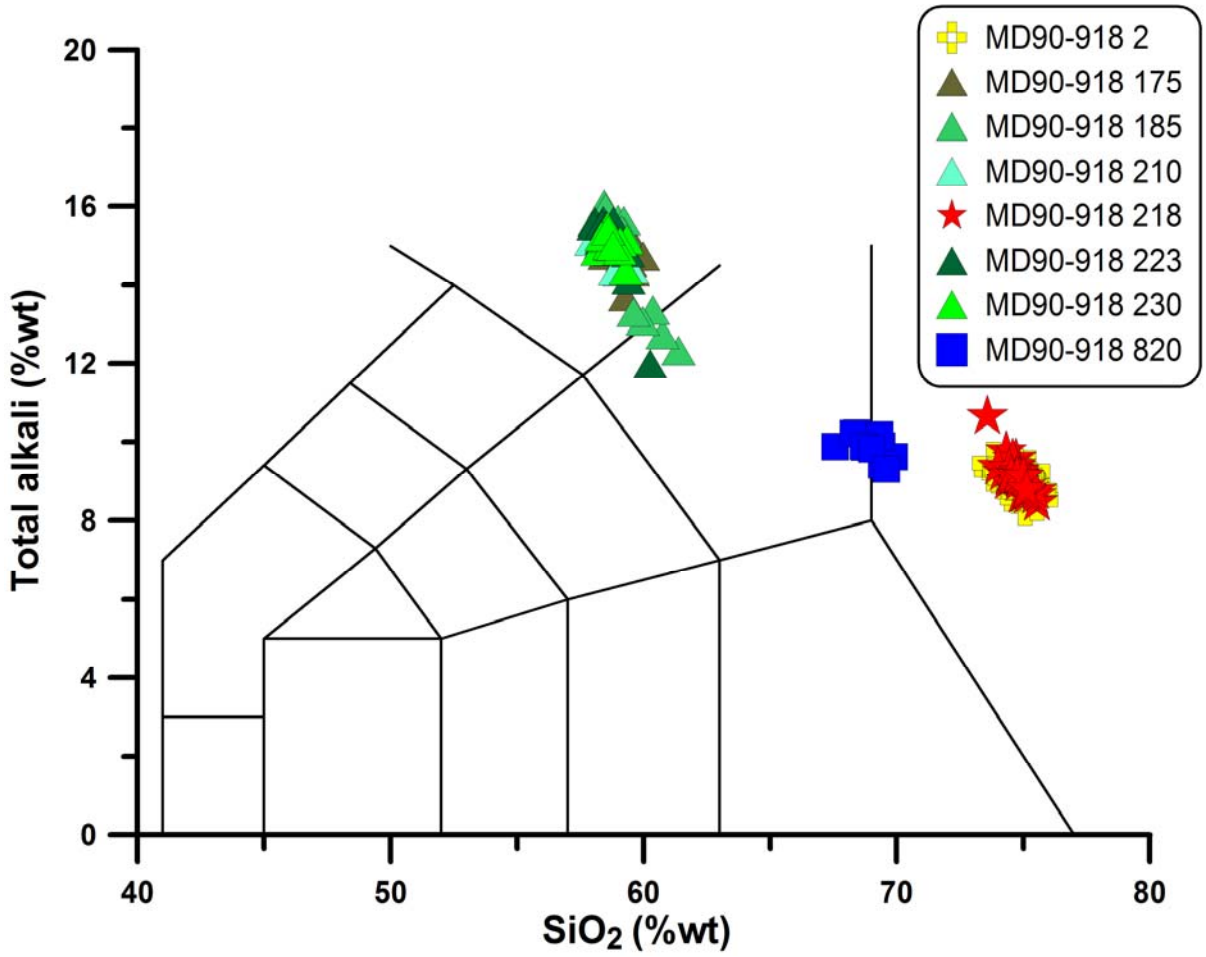
MD90-918 2
MD90-918 175
MD90-918 185
MD90-918 210
MD90-918 218
MD90-918 223
MD90-918 230
MD90-918 820
Total alkali (%wt)
SiO2 (%wt)
0
4
8
12
16
20
40
50
60
70
80

Fig.3

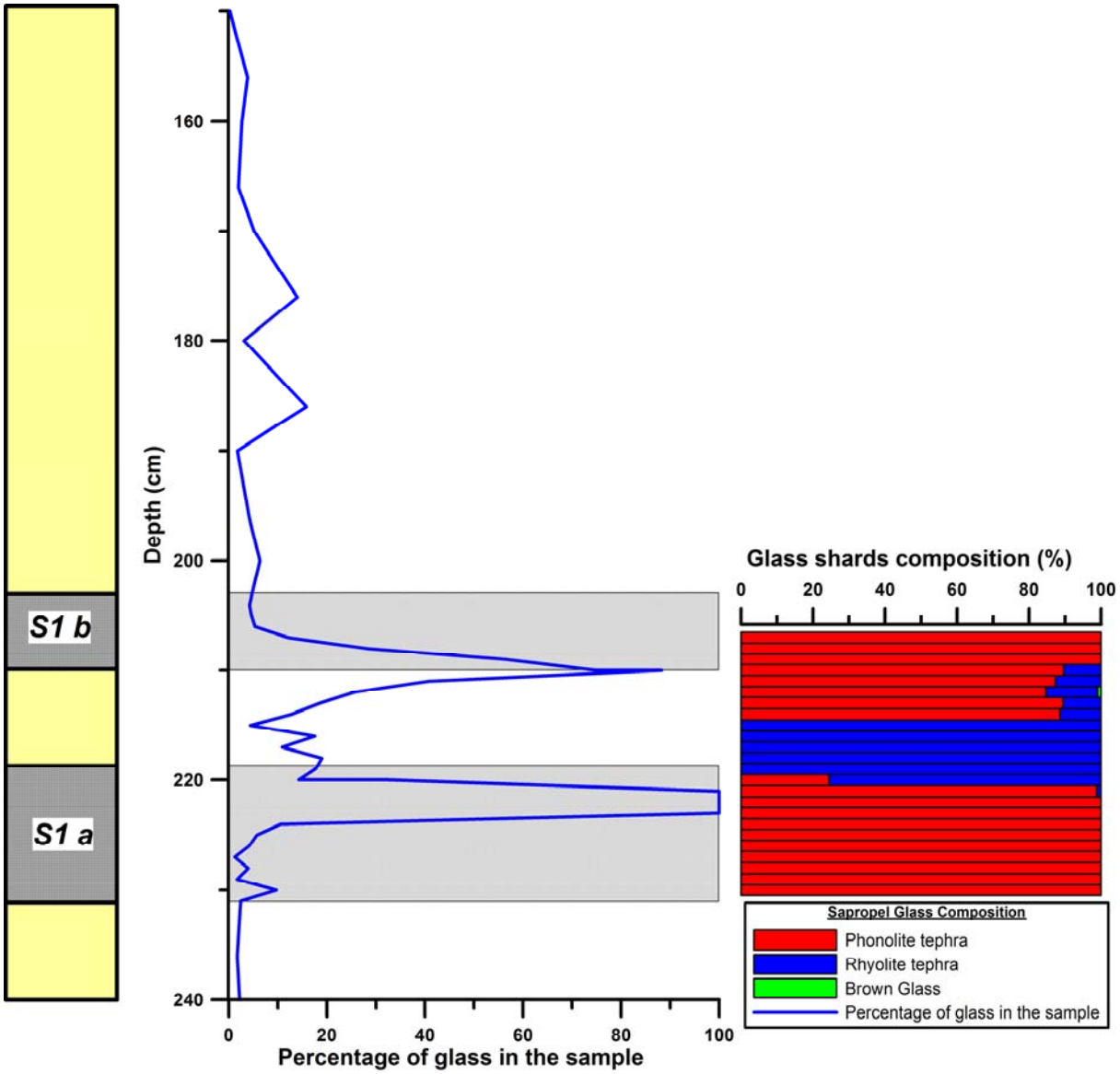
S1 b
S1 a
Depth (cm)
160
180
200
220
240
0
20
40
60
80
100
Percentage of glass in the sample
Glass shards composition (%)
0
20
40
60
80
100
Sapropel Glass Composition
Phonolite tephra
Rhyolite tephra
Brown Glass
Percentage of glass in the sample

Fig.4

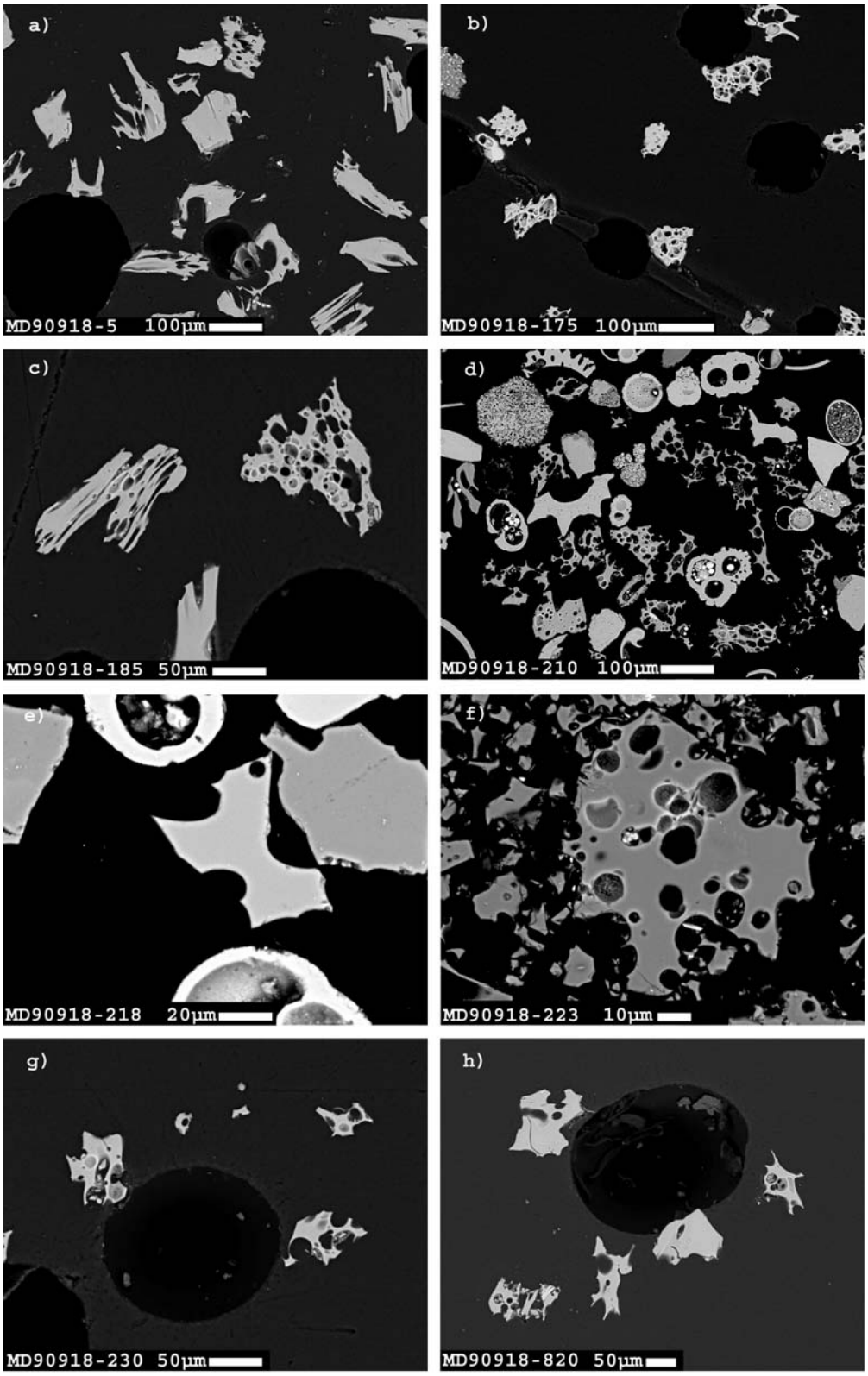
a)
MD90918-5 100µm
b)
MD90918-175 100µm
c)
MD90918-185 50µm
d)
MD90918-210 100µm
e)
MD90918-218 20µm
f)
MD90918-223 10µm
g)
MD90918-230 50µm
h)
MD90918-820 50µm
Fig.5

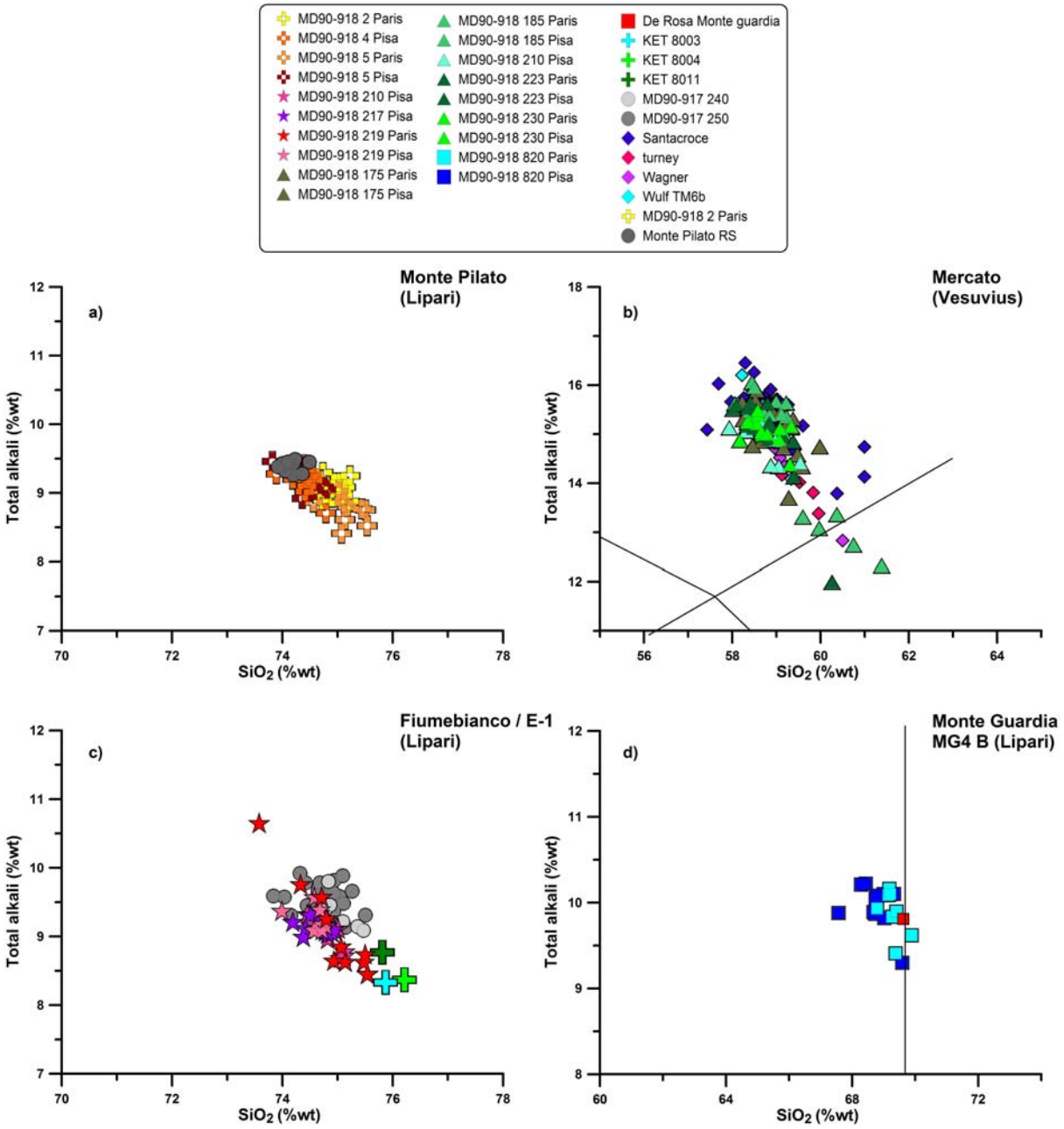
MD90-918 2 Paris
MD90-918 4 Pisa
MD90-918 5 Paris
MD90-918 5 Pisa
MD90-918 210 Pisa
MD90-918 217 Pisa
MD90-918 219 Paris
MD90-918 219 Pisa
MD90-918 175 Paris
MD90-918 175 Pisa
MD90-918 185 Paris
MD90-918 185 Pisa
MD90-918 210 Pisa
MD90-918 223 Paris
MD90-918 223 Pisa
MD90-918 230 Paris
MD90-918 230 Pisa
MD90-918 820 Paris
MD90-918 820 Pisa
De Rosa Monte guardia
KET 8003
KET 8004
KET 8011
MD90-917 240
MD90-917 250
Santacroce
turney
Wagner
Wulf TM6b
MD90-918 2 Paris
Monte Pilato RS
a)
Monte Pilato
(Lipari)
b)
Mercato
(Vesuvius)
c)
Fiumebianco / E-1
(Lipari)
d)
Monte Guardia
MG4 B (Lipari)
Total alkali (%wt)
SiO2 (%wt)

Fig.6

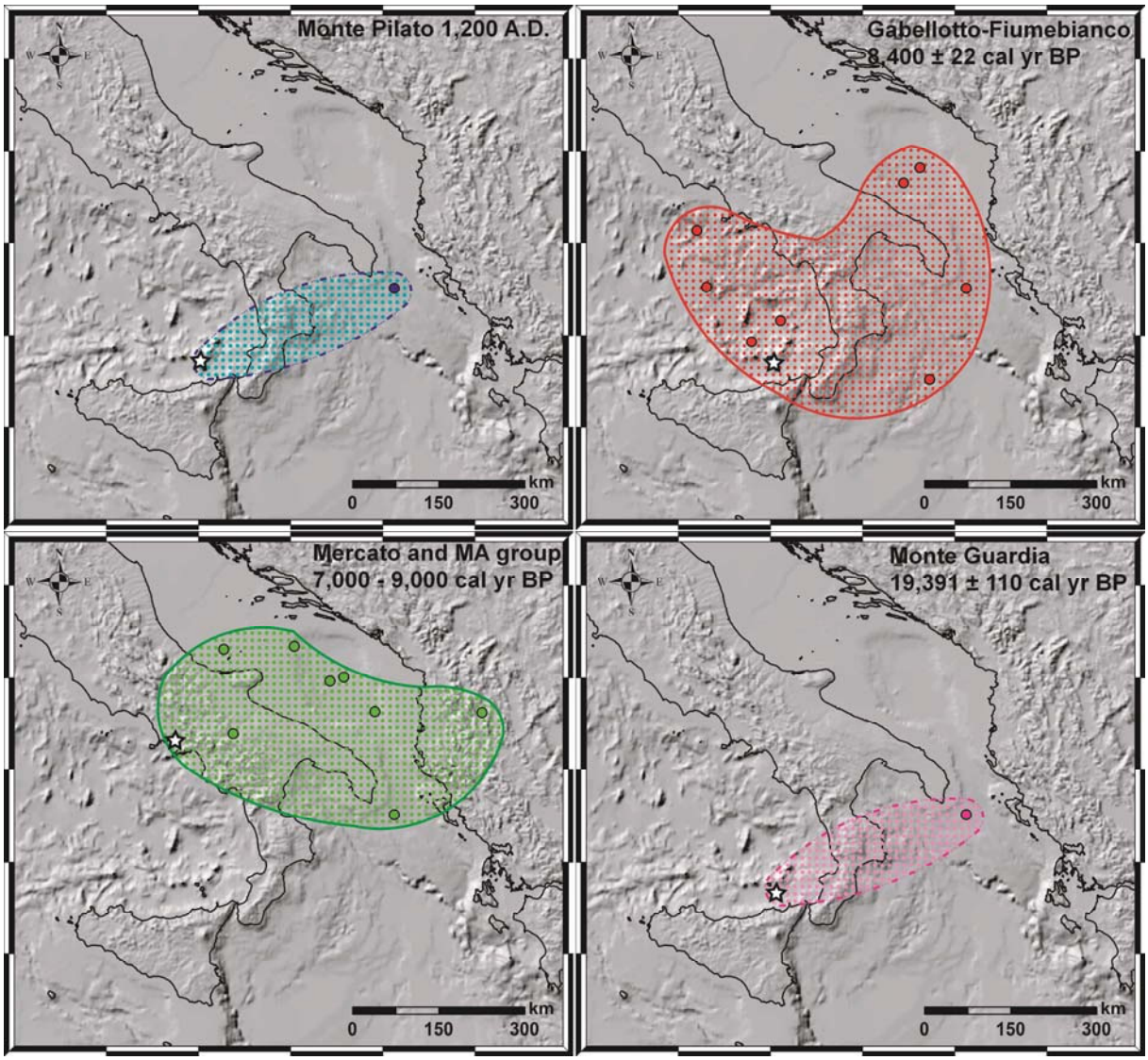
Monte Pilato 1,200 A.D.
Gabellotto-Fiumebianco
8,400 ± 22 cal yr BP
Mercato and MA group
7,000 - 9,000 cal yr BP
Monte Guardia
19,391 ± 110 cal yr BP
km
0
150
300
Fig.7

		SiO_2	TiO_2	Al_2O_3	FeO_{tot}	MnO	CaO	Na_2O	K_2O	ClO
Level 5	Mean of all analyses from the level 5	74.81	0.05	13.41	1.51	0.05	0.78	4.02	4.95	0.37
	Mean from the EPMA-CAMPARIS analyses	75.18	0.06	13.22	1.52	0.07	0.79	3.98	4.76	0.38
	Mean from the SEM-DST analyses	74.44	0.05	13.61	1.49	0.03	0.78	4.05	5.14	0.36
	Difference between the two means	0.74	0.01	-0.39	0.03	0.04	0.01	-0.07	-0.38	0.02
	Sd of the two means	0.52	0.01	0.27	0.02	0.03	0.00	0.05	0.27	0.01
	% variance of the two means from both instrument	**0.98**	**15.42**	**2.91**	**2.06**	**59.28**	**0.70**	**1.88**	**7.95**	**4.58**
Level 175	Mean of all analyses from the level 175	58.92	0.14	21.53	1.72	0.20	1.65	8.45	6.71	0.57
	Mean from the EPMA-CAMPARIS analyses	59.01	0.15	21.28	1.71	0.20	1.68	8.58	6.69	0.59
	Mean from the SEM-DST analyses	58.79	0.13	21.87	1.74	0.19	1.60	8.28	6.73	0.55
	Difference between the two means	0.22	0.03	-0.59	-0.03	0.01	0.08	0.30	-0.05	0.05
	Sd of the two means	0.16	0.02	0.42	0.02	0.01	0.05	0.21	0.03	0.03
	% variance of the two means from both instrument	**0.38**	**16.87**	**2.77**	**1.49**	**6.51**	**4.62**	**3.46**	**0.70**	**7.86**
Level 185	Mean of all analyses from the level 185	58.74	0.15	21.43	1.69	0.18	1.59	8.86	6.65	0.59
	Mean from the EPMA-CAMPARIS analyses	58.91	0.16	21.19	1.68	0.18	1.61	8.90	6.64	0.64
	Mean from the SEM-DST analyses	58.48	0.15	21.80	1.72	0.19	1.56	8.78	6.65	0.51
	Difference between the two means	0.43	0.01	-0.61	-0.04	-0.01	0.06	0.12	0.00	0.14
	Sd of the two means	0.30	0.01	0.43	0.03	0.01	0.04	0.08	0.00	0.10
	% variance of the two means from both instrument	**0.73**	**4.94**	**2.90**	**2.46**	**4.79**	**3.57**	**1.35**	**0.07**	**21.23**
Level 219	Mean of all analyses from the level 219	74.80	0.07	13.21	1.48	0.07	0.84	3.92	5.20	0.34
	Mean from the EPMA-CAMPARIS analyses	74.95	0.07	13.08	1.50	0.07	0.84	3.91	5.16	0.37
	Mean from the SEM-DST analyses	74.58	0.07	13.40	1.46	0.06	0.83	3.95	5.28	0.31
	Difference between the two means	-0.37	0.00	0.31	-0.04	-0.01	-0.01	0.04	0.13	-0.07
	Sd of the two means	0.26	0.00	0.22	0.03	0.01	0.01	0.03	0.09	0.05
	% variance of the two means from both instrument	**0.49**	**5.93**	**2.37**	**2.90**	**11.86**	**1.29**	**1.01**	**2.43**	**18.15**
Level 820	Mean of all analyses from the level 820	68.97	0.30	16.08	2.27	0.13	1.49	4.57	5.36	0.33
	Mean from the EPMA-CAMPARIS analyses	69.31	0.27	15.79	2.29	0.13	1.50	4.59	5.29	0.32
	Mean from the SEM-DST analyses	68.74	0.32	16.27	2.27	0.13	1.48	4.56	5.40	0.33
	Difference between the two means	0.57	-0.05	-0.48	0.02	0.01	0.02	0.03	-0.11	-0.01
	Sd of the two means	0.40	0.04	0.34	0.02	0.00	0.02	0.02	0.08	0.00
	% variance of the two means from both instrument	**0.82**	**20.18**	**3.03**	**1.05**	**5.11**	**1.61**	**0.68**	**2.07**	**1.82**
	average of the % variance	**0.68**	**12.67**	**2.80**	**1.99**	**17.51**	**2.36**	**1.68**	**2.65**	**10.73**

nb=99

Table1

Laboratorty Number	Core Depth (cm)	Species	^{14}C AMS age (yr BP)	± Error (yr)	Calibrated yr BP (range 1σ)	Source
SacA 15142	0-6	*G. ruber*	960	35	601-629	*intcal09*
SacA 15143	175-177	*G. ruber*	6535	45	6949-7029	*intcal09*
SacA 18291	215-217	*G. ruber*	7810	45	8237-8310	*intcal09*
SacA 15148	230-232	*G. ruber*	8470	50	8975-9034	*intcal09*
	300				11660	*Siani et al. 2010*
	420				14840	*Siani et al. 2010*
SacA 15149	470-472	*G. bulloides*	13740	60	16266-16724	*intcal09*
	590				17000	*Siani et al. 2010*
SacA 15150	820-822	*G. bulloides*	16610	70	19260-19465	*intcal09*
SacA 15151	1475-1477	*G. bulloides*	22710	110	27267-27513	*intcal09*

Table 2

MD90-918 2-Paris	SiO_2	TiO_2	Al_2O_3	FeO_{tot}	MnO	MgO	CaO	Na_2O	K_2O	P_2O_5	ClO	Total	Total Alkali	K_2O/Na_2O
3 / 1 .	75.14	0.09	13.14	1.27	0.03	0.05	0.79	4.09	4.99	0.00	0.39	100	9.08	1.22
5 / 1 .	75.02	0.14	13.02	1.37	0.06	0.06	0.81	3.81	5.33	0.02	0.36	100	9.15	1.40
6 / 1 .	75.23	0.00	12.88	1.49	0.10	0.04	0.67	3.83	5.42	0.02	0.32	100	9.25	1.41
7 / 1 .	75.09	0.21	12.95	1.51	0.04	0.04	0.76	3.88	5.12	0.00	0.40	100	9.01	1.32
8 / 1 .	74.57	0.01	13.40	1.46	0.13	0.03	0.87	3.90	5.22	0.03	0.37	100	9.12	1.34
9 / 1 .	74.93	0.00	13.07	1.61	0.06	0.05	0.78	3.96	5.18	0.02	0.33	100	9.15	1.31
10 / 1 .	75.03	0.00	13.07	1.63	0.07	0.05	0.74	4.01	5.04	0.00	0.36	100	9.06	1.26
11 / 1 .	74.73	0.27	13.06	1.39	0.07	0.04	0.76	3.82	5.48	0.00	0.37	100	9.30	1.43
12 / 1 .	75.21	0.05	13.09	1.49	0.12	0.04	0.75	3.98	4.89	0.00	0.37	100	8.88	1.23
14 / 1 .	74.73	0.01	13.49	1.62	0.06	0.05	0.77	4.02	4.87	0.02	0.37	100	8.89	1.21
16 / 1 .	74.90	0.02	13.23	1.54	0.11	0.05	0.81	3.73	5.21	0.00	0.40	100	8.94	1.40
17 / 1 .	74.78	0.15	13.26	1.53	0.09	0.04	0.78	3.83	5.15	0.03	0.36	100	8.98	1.34
18 / 1 .	74.69	0.01	13.27	1.58	0.06	0.05	0.77	3.97	5.21	0.01	0.38	100	9.19	1.31
19 / 1 .	75.00	0.02	13.14	1.57	0.05	0.05	0.75	3.90	5.07	0.04	0.39	100	8.98	1.30
mean	**74.93**	**0.07**	**13.15**	**1.50**	**0.07**	**0.05**	**0.77**	**3.91**	**5.16**	**0.01**	**0.37**	-	**9.07**	**1.32**
sd	**0.21**	**0.09**	**0.17**	**0.11**	**0.03**	**0.01**	**0.05**	**0.10**	**0.18**	**0.01**	**0.02**	-	**0.13**	**0.07**

MD90-918 4-Pisa	SiO_2	TiO_2	Al_2O_3	Fe_2O_3	MnO	MgO	CaO	Na_2O	K_2O	P_2O_5	ClO	Total	Total Alkali	K_2O/Na_2O
PI151-1	74.51	0.00	13.63	1.51	0.00	0.14	0.75	3.95	5.25	0.00	0.27	100	9.20	1.33
PI151-2	74.56	0.00	13.44	1.53	0.00	0.09	0.85	3.93	5.26	0.00	0.33	100	9.19	1.34
PI151-3	74.55	0.00	13.52	1.48	0.00	0.00	0.88	3.98	5.30	0.00	0.29	100	9.28	1.33
PI151-4	73.89	0.00	14.18	1.37	0.00	0.08	0.89	4.21	5.07	0.00	0.26	100	9.28	1.20
PI151-5	74.41	0.23	13.44	1.55	0.19	0.05	0.78	3.76	5.26	0.00	0.34	100	9.02	1.40
PI151-6	74.44	0.11	13.44	1.68	0.00	0.07	0.79	3.80	5.30	0.00	0.36	100	9.10	1.39
PI151-7	74.79	0.07	13.65	1.57	0.00	0.08	0.72	3.68	5.03	0.00	0.42	100	8.71	1.37
PI151-8	74.48	0.00	13.46	1.46	0.00	0.09	0.85	4.01	5.23	0.00	0.43	100	9.24	1.30
PI151-9	74.19	0.09	13.60	1.53	0.06	0.20	0.82	3.92	5.28	0.00	0.30	100	9.20	1.35
PI151-10	74.42	0.00	13.55	1.45	0.00	0.08	0.78	3.85	5.49	0.00	0.37	100	9.34	1.43
mean	**74.42**	**0.05**	**13.59**	**1.51**	**0.03**	**0.09**	**0.81**	**3.91**	**5.25**	**0.00**	**0.34**	-	**9.16**	**1.34**
sd	**0.24**	**0.08**	**0.22**	**0.08**	**0.06**	**0.05**	**0.06**	**0.15**	**0.13**	**0.00**	**0.06**	-	**0.18**	**0.06**

Table 3

Monte Pilato LIP22 cycle X	SiO_2	TiO_2	Al_2O_3	Fe_2O_3	MnO	MgO	CaO	Na_2O	K_2O	P_2O_5	ClO	Total	Total Alkali	K_2O/Na_2O
bulk rock	74.32	0.09	12.75	2.07	0.11	0.16	0.67	4.14	4.69	0.01	-	99.01	8.83	1.13
from Gioncada et al., 2003														
Monte Pilato PI-134	SiO_2	TiO_2	Al_2O_3	Fe_2O_3	MnO	MgO	CaO	Na_2O	K_2O	P_2O_5	ClO	Total	Total Alkali	K_2O/Na_2O
mean	74.16	0.12	13.51	1.58	0.21	0.05	0.76	4.07	5.32	0.00	0.34	-	9.39	1.31
sd	0.18	0.07	0.08	0.08	0.25	0.06	0.05	0.09	0.07	0.00	0.03	-	0.08	0.04
n=10, this work														
Mercato-Ottaviano	SiO_2	TiO_2	Al_2O_3	FeO_{tot}	MnO	MgO	CaO	Na_2O	K_2O	P_2O_5	ClO	Total	Total Alkali	K_2O/Na_2O
mean	59.45	0.10	22.12	1.75	0.21	0.09	1.59	7.95	6.11	0.00	0.62	-	14.06	0.77
sd	0.38	0.00	0.09	0.07	0.00	0.04	0.05	0.32	0.16	0.00	0.01	-	0.44	0.02
n=6, from Turney et al., 2008														
Mercato base TM-6b	SiO_2	TiO_2	Al_2O_3	FeO_{tot}	MnO	MgO	CaO	Na_2O	K_2O	P_2O_5	ClO	Total	Total Alkali	K_2O/Na_2O
mean	58.68	0.14	21.41	1.80	0.18	0.07	1.76	8.58	6.76	0.02	0.58	-	15.34	0.79
sd	0.30	0.03	0.21	0.13	0.03	0.01	0.25	0.18	0.54	0.02	0.04	-	0.55	0.07
n=10, from Wulf et al;, 2004														
Mercato base TM-6a	SiO_2	TiO_2	Al_2O_3	FeO_{tot}	MnO	MgO	CaO	Na_2O	K_2O	P_2O_5	ClO	Total	Total Alkali	K_2O/Na_2O
mean	60.06	0.31	20.53	2.26	0.12	0.16	2.48	5.41	8.11	0.05	0.50	-	13.53	1.55
sd	0.98	0.09	0.47	0.49	0.04	0.07	0.36	0.93	0.82	0.03	0.15	-	0.56	0.37
n=12, from Wulf et al., 2004														
Mercato	SiO_2	TiO_2	Al_2O_3	FeO_{tot}	MnO	MgO	CaO	Na_2O	K_2O	P_2O_5	ClO	Total	Total Alkali	K_2O/Na_2O
mean	58.82	0.13	21.81	1.77	0.14	0.09	1.66	8.60	6.97	-	0.53	-	15.49	0.82
sd	0.70	0.08	0.41	0.19	0.10	0.08	0.26	0.63	0.39	-	0.09	-	0.49	0.11
n=40, from Santacroce														
Mercato OT0702-2	SiO_2	TiO_2	Al_2O_3	FeO_{tot}	MnO	MgO	CaO	Na_2O	K_2O	P_2O_5	ClO	Total	Total Alkali	K_2O/Na_2O
mean	59.10	0.17	21.58	1.95	0.17	0.16	1.76	7.56	7.02	0.00	0.52	-	14.58	0.93
sd	0.55	0.09	0.13	0.11	0.07	0.09	0.13	0.56	0.27	0.00	0.03	-	0.83	0.48
n=9, from Vogel et al., 2009														

Table 4